Structure Analysis of a Fusogenic Peptide Sequence from the Sea Urchin Fertilization Protein Bindin†

Ralf W. Glaser, Matthias Grüne,‡ Christine Wandelt, and Anne S. Ulrich*

Institut für Molekularbiologie, Friedrich-Schiller-Universität Jena, Winzerlaer Strasse 10, D-07745 Jena, Germany

Received September 2, 1998; Revised Manuscript Received December 21, 1998

ABSTRACT: The structure of "B18", an 18-residue fusogenic peptide from the sea urchin fertilization protein bindin, was investigated in several membrane-mimicking environments with circular dichroism and nuclear magnetic resonance spectroscopy. The fully conserved peptide sequence represents the minimal functional part of the 24 kDa protein, which can bind to membranes and induce fusion of lipid vesicles. The B18 peptide undergoes a coil−helix transition in the presence of TFE, showing a transient tendency to self-associate. Its NMR structure in 30% TFE exhibits two helical regions at either side, connected by a flexible loop. In DPC and SDS detergent micelles, this loop becomes distinctly bent, presumably due to the high degree of curvature of the micelles. The loop contains a histidine-rich motif for binding zinc, which is required for the fusogenic function of the peptide. Therefore, we monitored the structural response of B18 and of recombinant bindin toward this ion. Like TFE, and in a mutually cooperative manner, zinc induces a partially helical structure in both the peptide and the protein. Complex formation via the histidine residues rigidifies the flexible loop and is accompanied by self-association of the molecules. The data suggest that the zinc-bound functional state is a continuous amphipathic α-helix, bearing some resemblance to a leucine zipper. Two hydrophobic patches on one face could favorably penetrate into a membrane, while two arginines on the other face could interact with lipid phosphate groups. The three-dimensional model of the B18 sequence thus contributes to a better understanding of peptide-induced vesicle fusion in general, and of the lipid−protein interactions of sperm bindin in particular.

Lipid−protein interactions during membrane fusion can be interpreted in the light of two complementary approaches. On one hand, an increasing number of crystal structures are being determined for viral and cellular fusion proteins, providing a unique and unifying picture about these fusion machineries (*1*, *50*). However, the crystal data contain no direct information about the membrane-interacting parts of the protein sequences as such. In an alternative approach, the fusogenic function of a protein can be reduced to its minimal active sequence, and the behavior of such a fusion peptide is then studied in the presence of lipid membranes (*2*). This kind of functional and conformational analysis, however, does not usually yield a detailed molecular structure of the peptide either. Since it is generally difficult to resolve structure and function of membrane-bound proteins, it is an acceptable compromise to perform high-resolution NMR[1] studies on model peptides in membrane-mimicking environments. For example, one of the few fusion peptides that have been resolved to date is the N-terminal sequence from HIV gp41 in SDS micelles (*3*). Here, we examine a putative fusion peptide from a sea urchin fertilization protein. Using NMR and CD spectroscopy under conditions that support the fusogenic activity of this particular model system, some intriguing structural analogies emerge from a comparison of the two unrelated but functionally similar peptides.

Sea urchin sperm bindin is a key protein in fertilization, constituting the major content of the acrosome granule (*4*, *5*). After its exposure on the sperm surface, the multifunctional protein mediates the species-selective gamete adhesion and presumably fusion with the egg membrane (*6*, *7*). Bindin has been shown to engage in a number of interactions: with itself, with lipid bilayers (*8*), with carbohydrate components of the egg vitelline envelope (*9*, *10*), and with Zn^{2+} ions (*11*). Sequence alignment among different sea urchin species (*12*−*15*) shows that the proteins share a central, highly conserved hydrophobic domain of 70−80 residues. The N- and C-terminal parts of the protein are strongly divergent and contain glycine- and proline-rich repeat elements.

Studies have been performed with tryptic fragments, deletion mutants, and synthetic peptides, to correlate the known functions of the protein with particular regions or sequence motifs. The relatively hydrophobic central part of bindin is responsible for its peripheral adhesion to lipid membranes (*16*, *17*). The protein triggers rapid fusion of vesicles consisting of sphingomyelin and cholesterol, lipids

† Financial support from the Deutsche Forschungsgemeinschaft (SFB 197/TP B13) and the Fonds der Chemischen Industrie (Liebig Stipendium).

* To whom correspondence should be addressed. E-mail: ulrich@molebio.uni-jena.de. Telephone: +49 3641 657572. Fax: +49 3641 657520.

‡ Present address: Max-Planck-Institut für Neurologische Forschung, Gleueler Strasse 50, D-50931 Köln, Germany.

[1] Abbreviations: B18, peptide sequence from sea urchin sperm bindin, numbered according to amino acids 103−120 of *Strongylocentrotus purpuratus*; Zn^{2+}, zinc ions; TFE, trifluoroethanol; NMR, nuclear magnetic resonance; CD, circular dichroism; SDS, sodium dodecyl sulfate; DPC, dodecyl phosphocholine; Δε, molar circular dichroic absorption difference; NOE, nuclear Overhauser effect; HN, amide proton; Hα, carbon α-proton.

10.1021/bi982130e CCC: $18.00
Published on Web 02/02/1999

that are known to be enriched in the outer leaflet of the plasma membrane (*18*). The conserved central sequence furthermore contains a histidine-rich motif, which is the Zn^{2+}-binding site of the native protein (*10*). The divergent hydrophilic terminal domains of bindin, on the other hand, mediate the species-specific recognition of the egg, via distinct carbohydrate patterns or via a proteinaceous sperm receptor (*7*, *19*−*21*). To rationalize the functions of bindin in the context of its three-dimensional molecular framework, structural studies are necessary, but they are severely hampered by self-association of the protein. Native bindin either is packaged into the acrosome granule or is available in a membrane-bound state, thus preventing both crystallization and high-resolution NMR investigations.

In an attempt to understand the interaction of native bindin with lipid membranes, we have focused our attention on an 18-residue peptide fragment from the central protein domain. The B18 sequence, LGLLLRHLRHHSNLLANI, which is fully conserved in all sea urchin species that have been studied, represents the minimal membrane binding and fusogenic motif of the native parent protein (*22*). It has been suggested to play a role similar to that of viral fusion peptides, in view of its analogous functional properties. The fusogenic activity of B18 is triggered by Zn^{2+}, according to fluorescence lipid mixing and vesicle leakage assays. Circular dichroism spectroscopy showed that Zn^{2+} induces a partially α-helical secondary structure in B18, leading to a distinct mode of self-association. In the absence of Zn^{2+}, the peptide is rapidly inactivated at pH ≥7, by aggregation into β-sheet amyloid fibrils. Using electron microscopy and X-ray diffraction, it was demonstrated that B18 can enter distinct folding pathways, which determine its functional state (*23*). An α-helical conformation is connected with its fusogenic activity toward uncharged large unilamellar vesicles, while a β-sheet structure is inactive and causes bilayer disruption.

Here, we investigate the three-dimensional structure of B18 in more detail, to determine those features that are relevant for membrane interaction, for Zn^{2+} binding, and for fusion. To perform NMR and CD measurements in solution, we used trifluoroethanol (TFE)/water mixtures as well as dodecylphosphocholine (DPC) and sodium dodecyl sulfate (SDS) micelles as membrane-mimicking environments. In addition, we evaluated the relevance of these peptide data for the structure−function relationship of the full-size bindin protein. These studies thus contribute to the general understanding of the molecular properties of fusogenic peptides, with potential implications for the mechanism of fertilization.

MATERIALS AND METHODS

Materials. The synthetic peptide B18 (LGLLLRHLRHHSNLLANI), representing amino acids 103−120 of the mature *Strongylocentrotus purpuratus* bindin sequence, was synthesized according to standard Fmoc protocols and purified with reverse phase HPLC. The peptide had free N- and C-termini. Lyophilized B18 was dissolved in bidest water, giving a slightly acidic stock solution (pH 4−5) in which the peptide was fully soluble at about 10 mg/mL for months. The peptide concentration was determined from methyl ^1H signals by NMR, calibrated against a known standard of leucine dissolved in H_2O.

Recombinant bindin was expressed in *Escherichia coli* with a plasmid (FpMb-5) containing the mature *S. purpuratus* sperm bindin sequence, connected to 31 residues of a λ cII gene product by a linker with the recognition sequence of factor Xa protease (*24*, *25*). The transfected strain was a gift from C. Glabe (University of California, Irvine, CA). The fusion protein is specifically cut by a bacterial protease during the purification procedure. The recombinant protein was purified as described by Lopez et al. (*26*).

Circular Dichroism Spectroscopy. CD spectra were recorded on a Jasco 710 spectropolarimeter with the following parameters: scan rate of 50 nm/min, step width of 0.5 nm, and response time of 1 s. A minimum of five scans per spectrum were accumulated. Spectra were recorded in BIS-Tris propane buffer (pH 7.5) at 5 °C, if not stated otherwise. Measurements of 5, 50, or 500 μM B18 were taken in a 10, 1, or 0.1 mm cuvette, respectively. Under these conditions, the molar circular dichroic absorption difference $\Delta\epsilon$ was calculated from the measured ellipticity θ with 1 mdeg = 0.337 M^{-1} cm^{-1} $residue^{-1}$.

Nuclear Magnetic Resonance Spectroscopy. NMR experiments were performed on a 500 MHz Varian Unity Inova spectrometer. Spectra of the following samples were analyzed: (i) "H_2O", 2.5 mM B18 in 90% H_2O/10% D_2O at pH 3 or 6.3; (ii) "TFE", 2.5 mM B18 in 30% TFE-d_3/63% H_2O/7% D_2O at pH 3 or 7, and <3 mM B18 and 20 mM phosphate buffer in 30% TFE/63% H_2O/7% D_2O at pH 7.5; (iii) "DPC pH 7.5", <3.5 mM B18, 175 mM fully deuterated dodecyl phosphocholine (DPC-d_{38}), and 160 mM phosphate buffer in 90% H_2O/10% D_2O at pH 7.5 [the latter two samples partially precipitated during the measurements; DPC-d_{38} was a gift from L. R. Brown (Jena, Germany)]; (iv) "DPC pH 3", 2.9 mM B18, 145 mM DPC-d_{38}, and 135 mM phosphate buffer in 90% H_2O/10% D_2O at pH 3 (this sample was obtained from sample iii after resolubilizing the precipitated material with HCl); and (v) "SDS", 2.0 mM B18 and 120 mM fully deuterated sodium dodecyl sulfate (SDS-d_{25}, Cambridge Isotopes) in 95% H_2O/5% D_2O at pH 7.5. The pH measurements were not corrected for the effects of TFE or D_2O.

Clean TOCSY spectra (*27*, *28*) were recorded with a mixing time of 50 or 100 ms, using WATERGATE water suppression (*29*) and an MLEV17 (*30*) mixing sequence. NOESY spectra (*31*, *32*) were recorded with a mixing time of 75, 150, or 300 ms, also using WATERGATE. For DQF-COSY spectra (*33*), presaturation of the water resonance was applied. Two-dimensional spectra were collected in the States mode with typically 400−600 increments in t_1 and 32−96 scans per increment. Fourier transformation and baseline correction were achieved in PROSA (*34*) on an SGI workstation. Chemical shifts were referenced against internal TSP.

Evaluation of NMR Spectra. Sequence-specific resonance assignments were made interactively with the computer program XEASY (*35*) according to standard procedures (*36*). TOCSY and COSY spectra were used to assign the individual resonances within amino acid spin systems, and sequential connections in NOESY spectra revealed the position of the spin system in the peptide sequence. Amino acid residues of B18 are numbered 103−120 according to their position in the *S. purpuratus* protein. Volumes of NOE cross-peaks and scalar coupling constants were extracted with SPSCAN (http://gaudi.molebio.uni-jena.de/~rwg/spscan). Scalar couplings between HN and Hα protons were determined

from in-phase splittings of NOESY cross-peaks (*37*) and from line shape comparison between TOCSY and DQF-COSY cross-peaks after convolution with an antiphase and in-phase stick pattern, respectively (*38*). Calculation of three-dimensional structures was performed by simulated annealing of molecular dynamics in torsion angle space with DYANA (*39*).

RESULTS AND DISCUSSION

Solubility in Aqueous Buffer. The major obstacle in the structure investigation of both bindin and the B18 peptide analogue is their low solubility under relevant conditions. Native sperm bindin from acrosomal granules can only be solubilized under strongly denaturing conditions such as >4 M urea or guanidine hydrochloride. When the denaturant is removed, the protein slowly precipitates, which might be connected with its function as a "molecular glue" (*6*). Recombinant bindin is slightly more soluble, but it also has a strong tendency to self-associate. The differences between native and recombinant bindin may be due to the presence of Zn^{2+} (*11*), or to a post-translational modification of five consecutive serines (*17*) in the native protein.

The B18 peptide is very soluble at slightly acidic pH, when the three histidines are protonated and the molecule carries five positive charges. At a physiologically relevant pH of seawater, however, B18 slowly precipitates in a concentration-dependent manner (*23*). CD measurements show a typical "random coil" spectrum between pH 3 and 9 before precipitation sets in (data not shown). NMR measurements confirm that the peptide is virtually unstructured in water up to pH 6. The Hα chemical shifts of the individual residues (Figure 2A) do not show significant deviations from the values of the amino acid in unstructured peptides (*40*, *41*). There are no medium-range NOEs that would suggest any particular secondary structure of B18 in water (data not shown).

TFE Induces α-Helical Structure in the B18 Peptide. Titration of B18 with increasing amounts of TFE induces a change from random coil to an α-helical structure (Figure 1). The maximum attainable degree of helicity depends both on pH and on peptide concentration. At pH 4, the CD spectra can be interpreted in terms of an equilibrium between two states, with a single isodichroic point at 203 nm (Figure 1A). The line shape differences are characteristic of a coil−helix transition for all peptide concentrations between 5 and 500 μM. At pH 6.5 and 7.5, a similar gradual structure formation is only observed for low concentrations of B18 (5 μM). Under those conditions, saturation of the helical content occurs at around 30% TFE, and increased pH favors an increased degree of helicity (Figure 1C). The CD signal at 222 nm reaches about half the value expected for a fully folded helix (*42*). With a high peptide concentration (500 μM) at pH 7.5, however, the titration with TFE is more complex (Figure 1B). The signal intensity at 222 nm, which is characteristic of the extent of α-helical structure, remains nearly constant between 10 and 20% TFE (Figure 1C). An intermediate state appears to exist under these conditions, bounded by two isodichroic points at around 200 and 208 nm. In the same range, between 5 and 25% TFE at pH 7.5, we recorded a significant light scattering (350 nm, 90°) with a maximum at 15% TFE. So we interpret the intermediate line shape in the CD measurements as an oligomeric species that is formed at higher peptide concentrations. The presence of small peptidic aggregates is generally known to reduce the signal intensity across the full spectral width due to light scattering and a shadowing effect (*43*). The isodichroic point at 200 nm coincides with zero signal intensity, which suggests an equilibrium between the precipitated intermediate and a soluble state with the same conformation. It is likely that the self-associated peptide has a secondary structure comparable to that of the TFE-induced soluble state, since their CD line shapes are proportional to one another. The same helical peptide conformation thus appears to be stabilized by intermolecular interactions as well as by higher concentrations of TFE.

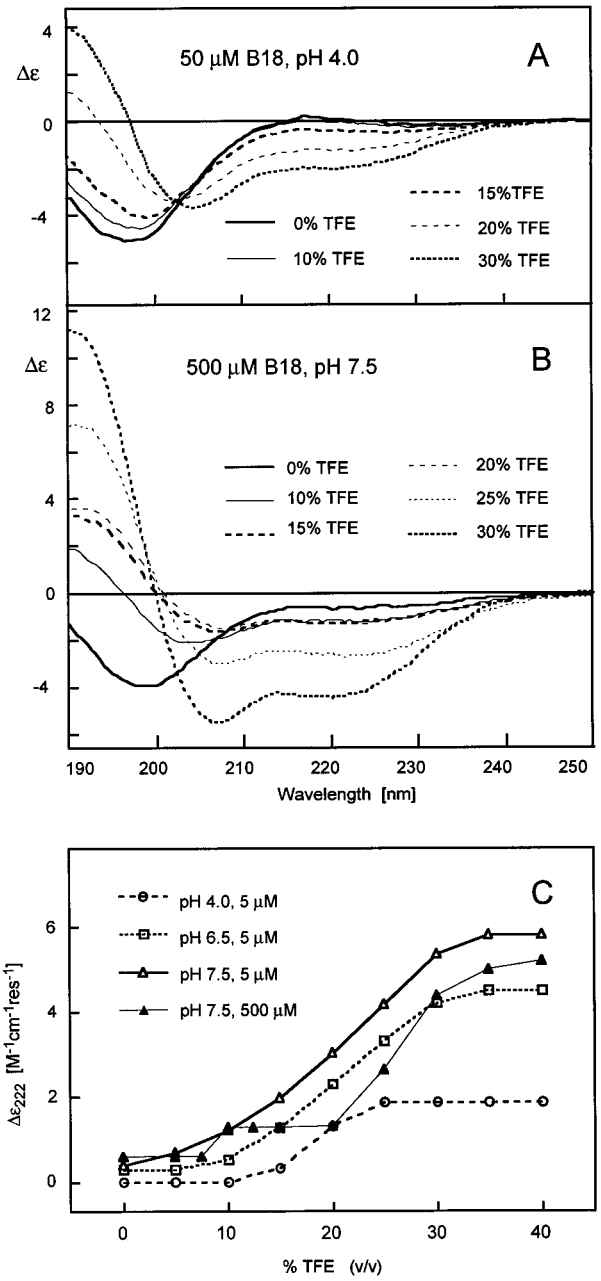

FIGURE 1: CD data for different concentrations of B18, titrated with TFE at different pHs, showing the formation of α-helical structure: (A) 50 μM B18 in 100 mM acetate buffer at pH 4.0, (B) 500 μM B18 in 100 mM BIS-Tris propane buffer at pH 7.5, and (C) specific CD absorption differences of B18 at 222 nm ($\Delta\epsilon_{222}$ in M^{-1} cm^{-1} $residue^{-1}$) as a function of TFE concentration.

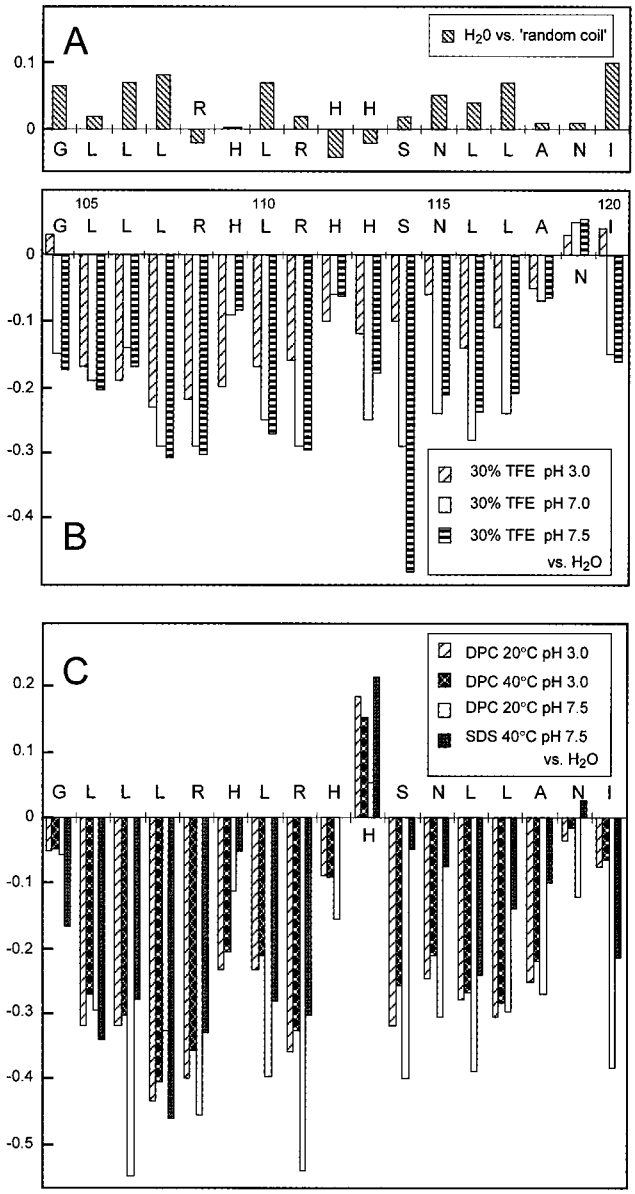

FIGURE 2: Comparison of NMR chemical shifts of α-protons in the peptide B18 under different conditions. (A) Hα chemical shifts of B18 in water at 7 °C and pH 3 (sample i), relative to the respective values of the residues of peptide GGXGG at 5 °C and pH 5 (*41*). (B) Hα chemical shifts of B18 in 30% TFE at 7 °C and pH 3 and 7, and at 20 °C and pH 7.5 (sample ii), relative to the values of B18 in water at pH 3. (C) Hα chemical shifts of B18 in the presence of DPC and SDS micelles in aqueous buffer. The exact composition of the samples is given in Materials. For the deprotonated histidines, a value of 0.25 ppm is added at pH ≥7 to account for the resulting intrinsic upfield shift.

While CD spectroscopy can provide a quick and qualitative estimate of secondary structure, the location of structural elements along the peptide backbone remains unknown. Having thus established the behavior of B18 under different conditions, we obtained a more detailed view of its structural preferences using homonuclear two-dimensional (2D) NMR spectroscopy. The chemical shifts, NOE patterns, and *J* coupling constants in 30% TFE are fully consistent with the predominantly α-helical conformation observed by CD. The Hα chemical shifts at pH 3, relative to those in water, suggest that the strongest tendency for helix formation resides in the N-terminal half of B18, between L105 and L110 (Figure 2B). At neutral pH and with 30% TFE, we find indications of an

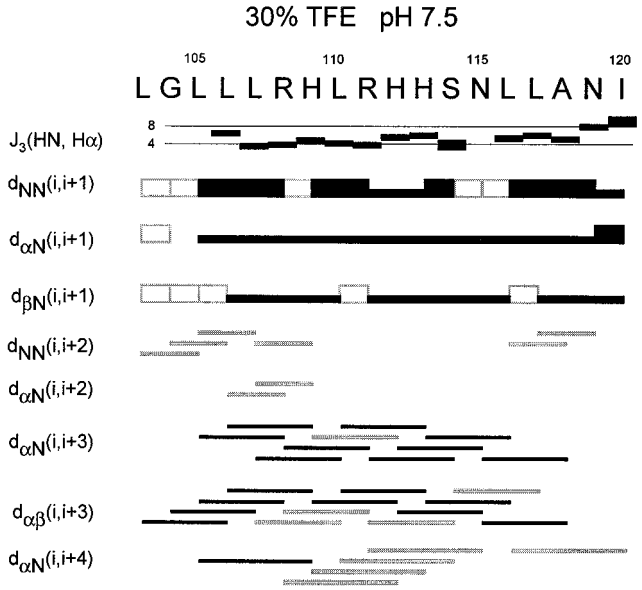

FIGURE 3: NMR *J* coupling constants and sequential and medium-range NOEs, observed for B18 in 30% TFE at 20 °C and pH 7.5. Coupling constants were determined by comparing the COSY and TOCSY line shapes of the HN−Hα cross-peaks (*38*). The position and thickness of the bar represent the *J* coupling value and its estimated accuracy, respectively; the two lines denote 4 and 8 Hz. Sequential NOE connections are shown as boxes with different heights for short- and medium-range NOEs. Light boxes represent connections where direct NOEs could not be unambiguously identified due to spectral overlap or strong spin diffusion or because one of the amide protons involved was not observed.

α-helical secondary structure in the complete peptide except for the terminal residues. Deprotonation of the three histidine side chains obviously facilitates helix formation at pH >6. In 30% TFE, all three histidines are fully deprotonated at pH ≥7, as indicated by their $H\epsilon_1$ chemical shifts. The Hα resonance of histidine in random coil peptides undergoes an upfield shift of about 0.25 ppm upon deprotonation (*40*, *41*). To distinguish this intrinsic effect from the structure-induced resonance shift, it was taken into account for the reference values. The average upfield shift of residues 104−118 in 30% TFE at pH 7.5 was 0.19 ppm relative to the chemical shifts of the respective residues in random coil peptides (*41*). If average upfield shifts of 0.3−0.4 ppm are assumed for a fully helical secondary structure (*44*), the resulting helicity of 50−60% for the 15-residue segment is in good agreement with the estimated helical content of the full peptide from CD spectra. Due to the lack of suitable reference values and the influence of factors other than secondary structure, however, such information obtained with either method should not be overestimated. It is consistent, nevertheless, with the pattern of sequential and medium-range NOEs and coupling constants (Figure 3) and indicates that in 30% TFE the peptide preferentially adopts an α-helical secondary structure, which is in fast exchange with other conformational states.

Structure calculations of B18 were carried out for 30% TFE at the physiologically relevant pH of 7.5 (Figure 4). The structure was determined on the basis of distance constraints derived from NOE cross-peaks and backbone ϕ dihedral angle constraints derived from HN−Hα scalar coupling constants. The calculations were performed with the program DYANA (*39*) with simulated annealing of

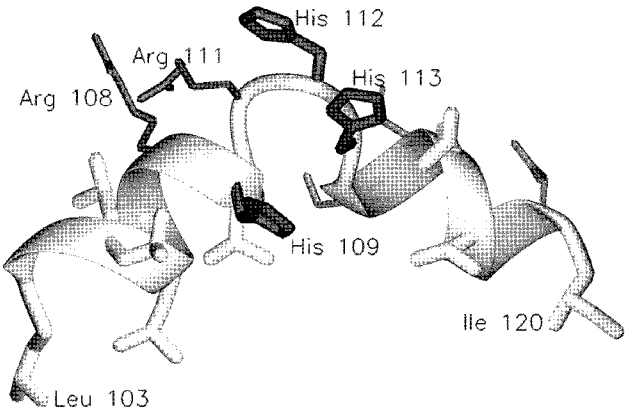

FIGURE 4: Characteristic structural features of the B18 peptide in 30% TFE at 20 °C and pH 7.5 showing two helical regions connected via a flexible hinge in the histidine-rich center. This representative structure with the lowest target function was selected from a set of 40 structures calculated with DYANA (*39*), using 177 upper limits, 14 coupling constants, and 239 lower-limit constraints (see the text). The figure was prepared with MOLMOL (*49*). Hydrophobic side chains (leucine and isoleucine) are thick white sticks; histidines are gray, and the remaining side chains are thin sticks.

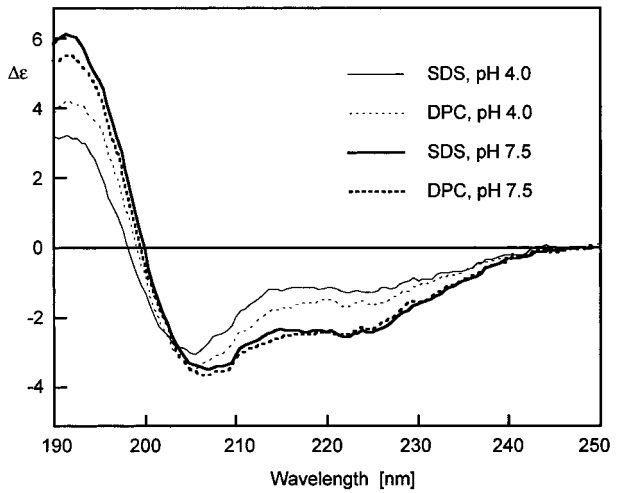

FIGURE 5: CD spectra of B18 in the presence of detergent micelles. Samples of 50 μM B18 with 1.6 mM sodium dodecyl sulfate (SDS, 1:32) or with 1.6 mM dodecylphosphocholine (DPC, 1:32) were measured in acetate buffer at pH 4.0 and in BIS-Tris propane buffer at pH 7.5. The spectrum of the detergent solution was subtracted.

molecular dynamics in torsion angle space. The calculations were repeated several times to assign some ambiguous NOE cross-peaks using preliminary structural information, and to test the influence of calibration parameters. The calibration of NOEs, i.e., the translation of NOE cross-peak volumes, v, into upper distance constraints, r, was a critical step in the calculation. Calibration with the standard "caliba" macro of the program DYANA did not provide a self-consistent set of constraints. This is not surprising as the peptide is expected to have internal motion and to undergo anisotropic tumbling. Under these conditions, calibration is to some extent a subjective decision, because it is not possible to use fixed intraresidual distances as a reference. To account for the flexibility, either the scaling factor A was enlarged, or all NOEs were calibrated with the equation $r = Av^{-1/4}$. Values of A that are too large lead to poorly defined sets of structures, while values that are too small lead to an increasing number of violated constraints. It was possible to find calibration parameters that resulted in a set of well-defined structures (average global backbone rmsd < 1 Å) with only moderate violations of constraints (DYANA target function < 8), but these structures are unreliable for the following reasons. (i) The well-defined structure is inconsistent with the assumption of internal flexibility that was made for NOE calibration, and (ii) removal of a randomly selected 10% of the constraints led to different structural details. Therefore, we used calibration parameters that provided a more heterogeneous set of structures, which was less sensitive to the removal of some constraints. We tested whether a subset of these structures could be excluded by introducing lower distance constraints. For protons or pseudoatoms that had a distance of less than 5 Å in at least half of the structures but gave no NOE cross-peak, lower distance limits of 3.5 Å were introduced. These did not reduce the conformational space significantly.

We checked whether some of the observed NOEs could be explained by intermolecular distances in a dimer or oligomer. Two approaches were used. From the final set of three-dimensional structures, a NOESY peak list was simulated with DYANA and compared with the experimental spectrum. The NOESY spectrum did not contain any peaks that were not expected from the set of monomeric structures. Second, NOE upper distance constraints that were violated in some of the structures were investigated. When interpreted as intermolecular distances, they did not suggest a consistent orientation of two or more peptide molecules with respect to each other. These negative results cannot prove that the peptide is a monomer, but they show that it is justified from the available data to interpret all NOEs as intramolecular.

We are aware that a calculation using the standard NMR approaches for determining relatively rigid high-resolution NMR structures cannot reveal in detail the conformational space that is explored by a highly dynamic peptide. However, we consider the structural features that were reproducibly obtained with different calibrations of distance constraints and different weights of the coupling constants as a useful approximation of the structural preferences of the B18 peptide. We found two distinct helical regions around Leu105−Leu110 and Asn115−Ala118. The first region was always an α-helix, while the second region showed characteristics of a 3_{10}-helix in some of the structures. The residues in the center of the peptide also had a slight tendency toward a helical conformation, but they appeared to be significantly less defined; in all structures, at least one of these residues showed a nonhelical conformation. The structure shown in Figure 4 is a representative example of these structural features. The overall conformation in TFE appears to be rather dynamic, which is consistent with the small size of the peptide (*42*).

The pattern of sequential and medium-range NOEs and the coupling constants (Figure 3) support a reduced stability of helical structure around the histidines rather than a defined turn. The data shown in Figures 3 and 6 were generated by inspection of the NOESY spectra with simulated peak lists that contained, in different colors, medium-range NOE peaks and all other possible NOE peaks compatible with the calculated set of structures. This was done to distinguish three types of connections: (black boxes) unambiguously assigned NOE cross-peaks, (gray boxes) ambiguous cross-peaks that

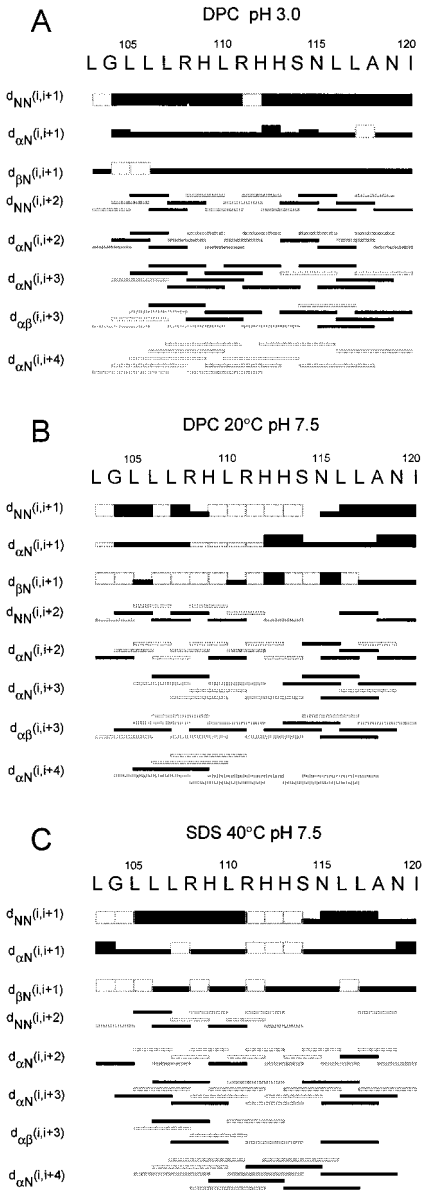

FIGURE 6: Sequential and medium-range NOEs observed for B18 in the presence of DPC and SDS detergent micelles. (A) B18 with 1:50 DPC at pH 3.0 (sample iv). NOESY spectra with mixing times of 75 and 150 ms at 40 °C and 150 ms at 20 °C were used. (B) B18 with 1:50 DPC at pH 7.5 and 20 °C (sample iii). (C) B18 with 1:60 SDS at pH 7.5 and 40 °C (sample v). Light boxes represent connections where direct NOEs could not be unambiguously identified due to spectral overlap or because an amide proton was not observed. The data in panel A, but not in panels B and C, were checked for spin diffusion.

could possibly result from overlap with other resonances as well as peaks that cannot be observed even if the distance between the protons is small, and (missing boxes) connections where no NOE cross-peaks were observed due to large distances.

B18 Forms a Helix−Break−Helix Motif with Detergent Micelles. Titration of B18 with the micelle-forming detergents DPC or SDS also induces a partially α-helical conformation, as monitored by CD spectroscopy (Figure 5). Folding is complete at a ratio of peptide:detergent molecules of about 1:30 to 1:40, the final degree of helicity being smaller than what was observed in TFE. A similar trend for facilitating helix formation with increasing pH is visible here, although the structural differences induced by the protonated and deprotonated states of the histidines are smaller. Remarkably, the anionic SDS has virtually the same effect as the neutral DPC on the secondary structure of the positively charged B18. It is thus conceivable that the peptide binding also to lipid bilayers will be driven mainly by hydrophobic interactions rather than by electrostatic attraction.

NMR experiments were carried out with three micellar samples as described in Materials: two B18 samples with 1:50 DPC-d_{38} at pH 7.5 and 3.0 and one sample with 1:60 SDS-d_{25} at pH 7.5. All three data sets showed the same basic structural features. The pattern of medium-range NOEs (Figure 6) and the Hα chemical shifts (Figure 2C) indicate two α-helical regions for L105−R111 and S114−A118. Slight differences are only found in the relative stabilities of the helical parts. If we interpret the average Hα chemical shifts quantitatively as a measure of helicity, the stability of the helical regions decreases with lower pH and with increasing temperature, as expected. We cannot explain why the average upfield shift of Hα resonances in DPC micelles is much larger than in SDS, while the CD spectra of the peptide in the presence of the two detergents are nearly identical. In SDS micelles, the C-terminal half of the peptide appears to be less helical than in DPC, as S114 and N115 have nearly the same chemical shift as in water, and two of the *i*,*i*+3 NOEs are weak or missing.

The combined NMR data in micelles show, together with the observed HN−Hα coupling constants J of >7 Hz for H113, consistently that a nonhelical conformation interrupts the helical peptide structure at residues H112 and H113; in this region, the helix is much more disturbed than in 30% TFE. Note, for instance, the pronounced downfield shift of Hα on H113 in contrast to all other residues on B18 (Figure 2C). Furthermore, the amide protons of H112 and L110 cannot be observed in the DPC sample at pH 7.5, and those of H112 are also missing in SDS at pH 7.5. Since the Hα resonances in these residues are not any broader than in the rest of the protein, we assume that the corresponding amide protons undergo very fast exchange with water. Consequently, they are neither involved in a stable hydrogen bond nor buried in the core of the micelle. Since residues R108−H113 carry two to five positive charges, depending on the pH, it is rather unlikely that the central part of B18 could be accommodated in the interior of a micelle. The leucine-rich termini of B18, on the other hand, are much more hydrophobic. A continuous rodlike α-helix would not, however, be able to interact favorably with a single micelle, regardless of whether the leucine-rich regions prefer an interaction via the micellar surface or an immersion into the interior. Therefore, it is tempting to speculate that the micelle forces the peptide to bend, thus inducing the observed break in the helix. The B18 NMR structure in 30% TFE had already provided some indication of a flexible hinge in this histidine-rich central region (Figure 4).

Despite the questionable relevance of a micellar environment as a model for a flat bilayer membrane, we characterized the structure of B18 in more detail. No long-range NOEs between residues more than five positions apart could be unambiguously identified. Although the narrow dispersion of leucine side chain resonances would make it difficult to identify any long-range NOEs if they existed, we believe that there are no defined contacts between the two helical

regions of the peptide. The structure calculations on the basis of NOE-derived distance constraints and HN−Hα coupling constants confirmed the helix−break−helix motif for all three micellar samples. Similar to the structure calculations for 30% TFE discussed above, we could obtain bundles of structures with low rmsd values (data not shown). However, we consider such apparently well-defined structures quite prone to artifacts, since the removal of a small number of constraints led to significant structural changes. Different conformations of the central region and different preferential orientations between the N- and C-terminal helices under various detergent, temperature, and pH conditions could be explained by a lack of certain constraints due to degenerate resonances, rather than an indication of significant qualitative or quantitative differences in NOE patterns.

It should be emphasized that all peaks in the NOESY spectra can be explained on the basis of simulated peak lists for a set of monomeric peptide structures, containing two helical regions and a short loop at histidines 112 and 113. These data are consistent with an angle of about 90−120° between the two helices. We conclude that the two terminal regions of B18 prefer a helical conformation, but the central region of the peptide possesses a distinct break in the micellar environment.

Zinc Ions Induce a Structural Change and Precipitation of Peptide. The native sperm bindin contains an equimolar amount of zinc, which must be bound by the histidines of the B18 sequence, as there are no cysteines and no other conserved histidines in the protein (*11*). The B18 peptide requires micromolar concentrations of Zn^{2+} to become fusogenic toward uncharged vesicles (*22*). The Zn^{2+} ions induce a partially helical secondary structure in B18, which is accompanied by oligomerization and subsequent precipitation (*23*). Since the Zn^{2+} binding is functionally important, we have monitored here the resulting conformational changes with CD under conditions comparable to those used in the experiments described above.

At a low peptide concentration of 5 μM, the addition of $ZnCl_2$ leads to a decrease of the CD signal intensity without much change in the line shape (Figure 7A). The peptide gradually starts to precipitate. At a high peptide concentration of 500 μM, on the other hand, a substoichiometric amount of Zn^{2+} already induces a structural change reminiscent of an α-helical conformation (Figure 7C). Remarkably, around a Zn^{2+}:peptide ratio of 1:1, the spectra are very similar to those of the helical B18 oligomer observed at an intermediate TFE concentration (Figure 1B, 15 and 20% TFE). In the presence of excess Zn^{2+}, the peptide then starts to precipitate visibly, and the CD signal intensity decreases accordingly. For an intermediate peptide concentration of 50 μM, the final spectrum of the B18−Zn^{2+} precipitate is similar to that at 500 μM, but it is approached via a direct route with a single isodichroic point at around 210 nm (Figure 7B).

It would have been desirable to record NMR spectra of B18 with bound zinc, but it was not possible to produce stable soluble B18−Zn^{2+} complexes in aqueous buffer at pH 7.5. At a Zn^{2+}:peptide ratio of 1:2 and an initial peptide concentration of 1 mM, most of the material precipitates within a few hours. Nevertheless, it is possible to draw structural conclusions from the CD data alone, given that the spectra of B18 with a stoichiometric amount of Zn^{2+} (Figure 7C) are virtually identical to those of B18 in 15−20% TFE (Figure 1B). These line shapes furthermore have the same proportions as the soluble B18 in 30% TFE (Figure 1B). Their only difference appears to lie in the degree of self-association which causes differerential degrees of light scattering. From the analogy of these data, we conclude that the peptide conformation in the oligomeric Zn^{2+} complex resembles not only the self-associated but also the soluble α-helix in TFE, whose structure has been determined with NMR (Figure 4).

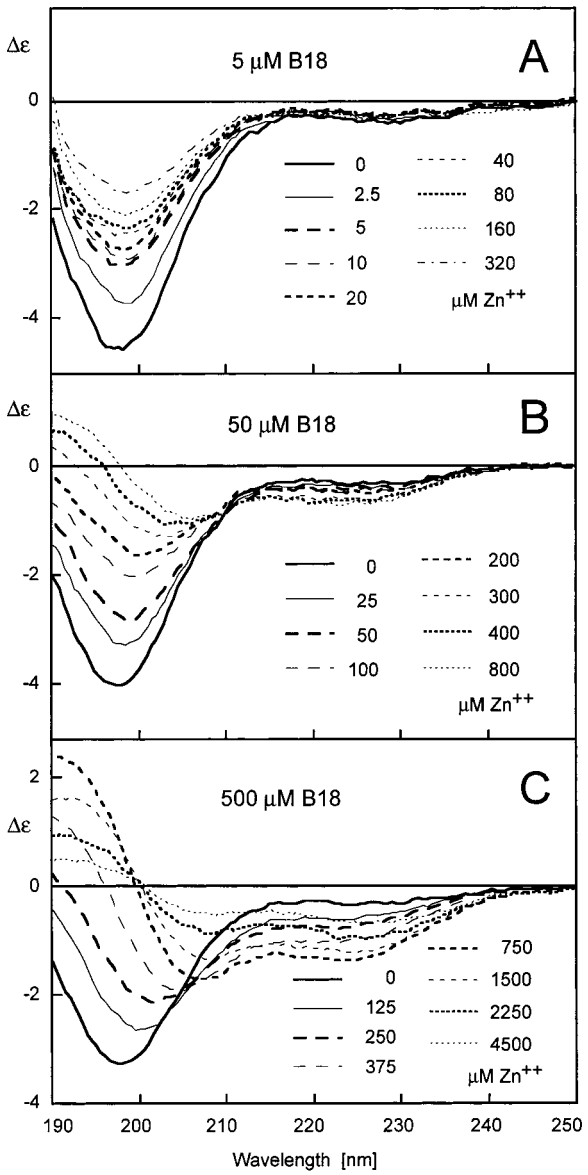

FIGURE 7: CD spectra of B18 upon the addition of $ZnCl_2$ in BIS-Tris propane buffer at pH 7.5: (A) 5 μM B18, (B) 50 μM B18, and (C) 500 μM B18. The concentration of Zn^{2+} ions is indicated for the individual spectra in the figure.

TFE and Zn^{2+} Cooperatively Lead to an Amphipathic α-Helix of B18. Qualitatively similar changes in the CD spectra are induced by Zn^{2+} and TFE, as discussed above. This observation is further supported by a cooperative structural effect of Zn^{2+} and TFE, which is particularly obvious at pH values around the p*K* of the histidines. For example, neither 10% TFE nor 0.5 equiv of Zn^{2+} (250 μM) has, on its own, any significant influence on the random coil structure of 500 μM B18 in BIS-Tris propane buffer at pH 7.0. When 0.5 equiv of Zn^{2+} is combined with the presence

of 10% TFE, however, they are able to induce a significantly α-helical CD spectrum (data not shown). The resulting structure is, once more, very similar to that of the oligomeric intermediate obtained either with an equimolar amount of Zn^{2+} or with 15−20% TFE at pH 7.5 (see the discussion above). When we start with this intermediate oligomeric structure, the addition of more Zn^{2+} leads to precipitation, as expected. Addition of more TFE, on the other hand, increases the intensity of the helical CD signal, again consistent with the solubility of B18 at high TFE concentrations observed above.

We did not find any cooperative effect between Zn^{2+} and detergent micelles. Addition of Zn^{2+} to B18 preincubated with SDS did not change the CD spectrum. Addition of SDS to the peptide preincubated with Zn^{2+} had the same effect as if SDS was added to a reduced amount of B18 alone, since the Zn^{2+}-precipitated peptide was not solubilized by SDS (data not shown). These CD results may have two possible interpretations. Either the SDS-bound conformation of the peptide is unable to interact with Zn^{2+}, or the conformation of the peptide backbone in the micelle does not change upon binding of Zn^{2+}. The distinct break in the helical structure around the histidine residues, observed in the NMR analysis with detergent micelles, supports the first interpretation.

Due to steric crowding of the histidines in the motif HxxHH, it is likely that the Zn^{2+} ion is bound by only two out of the three residues on one peptide (*22*). It is well-known that an α-helical structure is stabilized by complex formation between two histidines in positions i and $i + 4$ (*45*). This structural preference explains the cooperative effect of Zn^{2+} and TFE. TFE favors the formation of α-helical structure mainly in the hydrophobic regions on both sides of the peptide, and to a lesser extent in the center. In a complementary way, Zn^{2+} binding induces an α-helical loop in the center of B18, which may act as a nucleation site for further folding.

Under functionally relevant conditions, B18 binds to a lipid membrane in the presence of Zn^{2+}. We suggest that B18 then forms a relatively stable α-helix over the full length of the peptide. In a continuous α-helix, both hydrophobic patches of B18 are oriented on the same face, as illustrated in Figure 8. An equivalent three-dimensional picture may also be visualized by inspection of Figure 4, provided that the central kink is being straightened out. This amphiphilic structure would allow a favorable penetration of the hydrophobic face of B18 into a membrane, with the two arginine side chains positioned on the opposite side. Overall, a partial immersion of the peptide between the lipids is expected to lead to bilayer destabilization and vesicle fusion. The proposed structure of B18 is also vaguely reminiscent of a leucine zipper (Figure 8), which could explain its mode of self-association via hydrophobic surfaces.

Analogous Structural Response of the B18 Peptide and Bindin. Previous studies have shown functional analogies between B18 and the parent protein bindin, concerning their interaction with membranes. Both bind to lipid bilayers and induce vesicle fusion, and both seem to require Zn^{2+} for their integrity and function (*11*, *22*). The following question arises. To which extent are the structural studies on B18 relevant for understanding the structure and function of sea urchin bindin during fertilization? Therefore, the qualitative structural features of the full-size protein are investigated here using CD, and they reveal significant analogies to B18. Recombinant bindin (236 amino acids) was freshly dissolved in water after the removal of denaturing agents by dialysis. The protein possesses a predominantly random coil conformation, with some degree of secondary structure according to the signal intensity at 222 nm (Figure 9A). Upon the addition of Zn^{2+} ions at pH 7.5, the recombinant bindin undergoes a conformational change toward a more helical structure, just as was observed for the B18 peptide (cf. Figure 7C). The increase in negative intensity of $\Delta\epsilon_{222}$ by about 1 M^{-1} cm^{-1} $residue^{-1}$ shows that at least 10% of the 236 residues are involved in the change. In the presence of excess Zn^{2+}, bindin eventually precipitates from the solution (Figure 9B,C). This kind of Zn^{2+}-induced self-association is again reminiscent of the behavior of B18, although in the case of bindin some β-sheet structure appears to be added in this process (which is difficult to quantitate due to strong light scattering). According to our studies on B18, these observations may be explained by two different mechanisms. A local α-helical conformation is formed by the binding of Zn^{2+} to histidines H109 and H113, which may act as a folding nucleus. Alternatively, Zn^{2+} may form a bridge between two bindin molecules, and structure formation is then induced by intermolecular contacts. Further oligomerization and precipitatation of the protein are consistent with the highly self-associated state of native bindin.

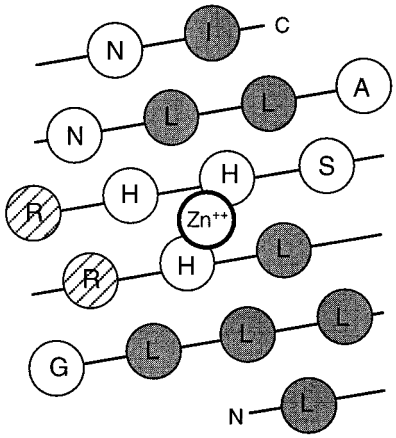

FIGURE 8: Schematic representation of B18 as a continuous α-helix, showing two hydrophobic patches on one face (shaded residues). The charged arginines are located on the opposite face. Histidine residues H109 and H113 in positions i and $i + 4$ have been identified to bind the Zn^{2+} ion (L. Magdaleno et al., unpublished).

The α-helical content of recombinant bindin was found to increase also in the presence of TFE (data not shown). About 20% TFE was sufficient to induce a helicity at 222 nm comparable to that observed with 200 μM Zn^{2+} (cf. Figure 9A). Increasing the TFE concentration up to 50% induced little further change. However, compared to the highly localized action of Zn^{2+}, the effect of TFE in favoring a helical secondary structure is rather unspecific. Therefore, we have no indication that the observed response is related to structural changes in the central part of bindin. The addition of SDS or DPC micelles to recombinant bindin does not induce any significant changes in the CD spectrum. This is not too surprising if we consider that bindin, in contrast to B18, has a much more selective interaction with lipid membranes (*23*). The protein preferentially binds to phos-

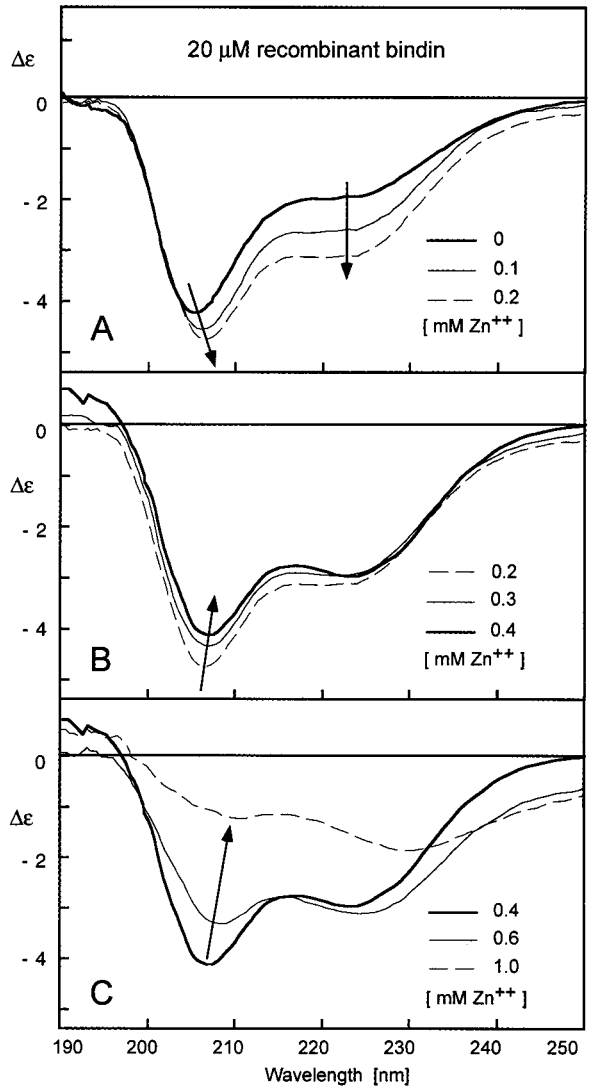

FIGURE 9: CD spectra of recombinant bindin upon the addition of $ZnCl_2$. Bindin (20 μM) was titrated with 0−1 mM Zn^{2+} in Tris buffer at pH 7.6. The successive changes in the line shape and the reversal in signal intensity are illustrated in separate panels (A−C). At 0.6 and 1 mM $ZnCl_2$, the spectrum has large baseline artifacts resulting from light scattering of the precipitating protein.

phatidylcholine membranes in the gel phase, and it rapidly fuses sphingomyelin/cholesterol vesicles (*8*), whose topology bears little resemblance to that of fluid detergent micelles.

Overall, significant structural and functional similarities are evident for B18 and bindin, but the limitations of B18 as a model are also obvious. The free peptide possesses a much higher conformational freedom compared to an internal sequence of a protein. Furthermore, the remaining parts of bindin will engage in additional interactions with the membrane, with other proteins, and with carbohydrates. The mode of intermolecular interaction between B18 peptide molecules and between bindin protein molecules must also be different, because steric hindrance by the bulky hydrophilic domains of bindin would probably prevent the direct contact of large numbers of B18 sequences in a protein aggregate. Nevertheless, the full-size protein responds to Zn^{2+} ions, pH (histidine protonation), and environmental conditions in a manner similar to that of the isolated B18 peptide.

Structure−Function Relationship of the B18 Sequence. Sea urchin bindin plays a multifunctional role in fertilization, by moderating the species-specific adhesion and presumably membrane fusion between sperm and egg. The B18 peptide has been identified as its minimal membrane binding sequence, and it has been suggested that it acts as a fusion peptide. This proposal was based on lipid mixing assays and electron microscopy, showing that B18 is able to induce extensive fusion between large uncharged unilamellar liposomes in vitro (*22*, *23*). To rationalize the behavior of B18 in the light of other fusogenic proteins, among which viral systems are the most thoroughly studied examples, the common structural features in a membranous environment are of interest. Many fusogenic peptides show a correlation between activity and α-helical conformation, although others are implicated as acting like a β-sheet structure (*2*). It has been postulated that an important requirement for fusion activity is a high conformational flexibility (*46*). A critical feature might be the ability of a disordered peptide to fold into an amphipathic structure once it is close enough to the membrane, without being trapped in an unsuitable location or conformation beforehand.

In the case of B18, we have observed an amphipathic α-helical conformation, which is relatively flexible around the histidine residues in its center, when measured in 30% TFE (Figure 4). Binding of a Zn^{2+} ion, which is necessary for the fusogenic activity of B18, probably results in a continuous α-helix with two hydrophobic patches on the same face, which would allow a favorable binding to the membrane. Two arginine side chains point the other way and may engage in further electrostatic interactions with the lipid phosphate groups (Figure 8). Detergent micelles, on the other hand, induce a pronounced bend in the center of the peptide, and appear not to be a suitable model for the interaction of B18 with lipid bilayers. Nevertheless, the detergent data suggest that the affinity of B18 for a membrane is driven predominantly by hydrophobic interaction rather than by charge. In the absence of a suitable membrane-mimicking environment, Zn^{2+} binding is accompanied by extensive self-association between the α-helical peptides, suggesting an intermolecular stabilization of its hydrophobic surfaces.

As a mechanism for fusion, an oblique insertion of helical peptides into the lipid bilayer has been proposed (*47*). In the case of B18, it is not obvious from our data whether either of the two hydrophobic ends would be preferentially immersed into the membrane. We note, however, that unlike most of the viral N-terminal fusion peptides investigated so far, the B18 sequence is connected at both ends to the parent protein. Even though the sequence of B18 is not homologous with any internal viral fusion peptides, such internal motifs might require a different evaluation of their fusion mechanism than terminal ones. If only an adhesive rather than a fusogenic function were attributed to the B18 sequence in the full-size bindin after all, a peripheral membrane attachment would be consistent with the amphiphilic character of the α-helix proposed here.

Besides conformational requirements, a necessity for oligomerization has been postulated for many fusion peptides as well as for their parent proteins. In this sense, B18 and bindin fit into the current picture of an adhesion and fusion machinery. On the other hand, a sequence comparison with different families of enveloped viruses shows no homologies, and we note that bindin does not possess a transmembrane

anchor, unlike viral and cellular fusion proteins. From the limited sequence data available, it appears that the properties of the conserved B18 motif, with the two central charged residues and the ability to bind Zn^{2+}, are unique to the sea urchin system.

A recent NMR study of the HIV gp41 fusion peptide in SDS micelles has shown that its N-terminal part assumes a helical structure in the hydrophobic core of the micelle, while the C-terminus is bent away to lie on the surface (*3*). The kink coincides with a highly conserved FLG motif, which has been implicated as a folding nucleus in an aqueous environment (*48*). It was suggested that the bend in SDS could easily be straightened to give a continuous α-helix, which might not be too unreasonable in view of the high degree of curvature of the micelles. When modeled as a straight α-helix, the FLG motif in HIV forms part of a glycine-rich patch, which is also found in several other fusion peptides and has been suggested to facilitate helix packing in self-associated peptides (*2*). A possible analogy might be drawn here with the structure of B18. It also possesses a flexible hinge that can be straightened to give a functionally active amphipathic helix. This folding also favors self-association, via hydrophobic surfaces and possibly via Zn^{2+} bridges.

ACKNOWLEDGMENT

We gratefully acknowledge Charles Glabe (University of California, Irvine, CA) for synthesizing the B18 peptide and for providing the vector for expressing recombinant bindin. We also thank Jochen Flemming (University of Jena, Jena, Germany) for helping with the NMR analysis.

REFERENCES

1. Binley, J., and Moore, J. P. (1997) *Nature 387*, 346−348.
2. Durell, S. R., Martin, I., Ruysschaert, J.-M., Shai, Y., and Blumenthal, R. (1997) *Mol. Membr. Biol. 14*, 97−112.
3. Chang, D.-K., Cheng, S.-F., and Chien, W.-J. (1997) *J. Virol. 71*, 6593−6602.
4. Vacquier, V. D., and Moy, G. W. (1977) *Proc. Natl. Acad. Sci. U.S.A. 74*, 2456−2460.
5. Glabe, C. G., and Vacquier, V. D. (1977) *Nature 267*, 836−838.
6. Vacquier, V. D., Swanson, W. J., and Hellberg, M. E. (1995) *Dev., Growth Differ. 37*, 1−10.
7. Hofmann, A., and Glabe, C. (1994) *Semin. Dev. Biol. 5*, 233−242.
8. Glabe, C. G. (1985) *J. Cell Biol. 100*, 794−799.
9. DeAngelis, P. L., and Glabe, C. G. (1988) *Biochemistry 27*, 8189−8194.
10. DeAngelis, P. L., and Glabe, C. G. (1990) *Biochim. Biophys. Acta 1037*, 100−105.
11. DeAngelis, P. L., and Glabe, C. G. (1990) *Pept. Res. 3*, 62−68.
12. Gao, B., Klein, L. E., Britten, R. J., and Davidson, E. H. (1986) *Proc. Natl. Acad. Sci. U.S.A. 83*, 8634−8638.
13. Minor, J. E., Fromson, D. R., Britten, R. J., and Davidson, E. H. (1991) *Mol. Biol. Evol. 8*, 781−795.
14. Glabe, C. G., and Clark, D. (1991) *Dev. Biol. 143*, 282−288.
15. Metz, E. C., and Palumbi, S. R. (1996) *Mol. Biol. Evol. 13*, 397−406.
16. Kennedy, L., DeAngelis, P. L., and Glabe, C. G. (1989) *Biochemistry 28*, 9153−9158.
17. Miraglia, S. J., and Glabe, C. G. (1993) *Biochim. Biophys. Acta 1145*, 191−198.
18. Miraglia, S. (1993) Ph.D. Thesis, University of California, Irvine, CA.
19. Minor, J. E., Britten, R. J., and Davidson, E. H. (1993) *Mol. Biol. Cell 4*, 375−387.
20. Just, M. L., and Lennarz, W. J. (1997) *Dev. Biol. 184*, 25−39.
21. Mauk, R., Jaworski, D., Kamei, N., and Glabe, C. G. (1997) *Dev. Biol. 184*, 31−37.
22. Ulrich, A. S., Otter, M., Glabe, C. G., and Hoekstra, D. (1998) *J. Biol. Chem. 273*, 16748−16755.
23. Ulrich, A. S., Tichelaar, W., Förster, G., Zschörnig, O., Weinkauf, S., and Meyer, H. W. (1999) *Biophys. J.* (submitted for publication).
24. Nagai, K., and Thogerson, H. C. (1984) *Nature 309*, 810−812.
25. Glabe, C. G., Brockman, S., Lopez, A., Kimura, K., Kennedy, L., and DeAngelis, P. L. (1989) in *Techniques in Protein Chemistry* (Hugli, T. E., Ed.) pp 448−455, Academic Press.
26. Lopez, A., Miraglia, S. J., and Glabe, C. G. (1993) *Dev. Biol. 156*, 24−33.
27. Bax, A., and Davis, D. G. (1985) *J. Magn. Reson. 65*, 355−360.
28. Griesinger, C., Otting, G., Wüthrich, K., and Ernst, R. R. (1988) *J. Am. Chem. Soc. 110*, 7870−7872.
29. Piotto, M., Saudek, V., and Sklenar, V. (1992) *J. Biomol. NMR 2*, 661−666.
30. Levitt, M. H., Freeman, R., and Frenkiel, T. (1982) *J. Magn. Reson. 47*, 328−330.
31. Jeener, J., Meier, B. H., Bachmann, P., and Ernst, R. R. (1979) *J. Chem. Phys. 71*, 4546−4553.
32. Kumar, A., Wagner, G., Ernst, R. R., and Wüthrich, K. (1981) *J. Am. Chem. Soc. 103*, 3654−3658.
33. Rance, M., Sorenson, O. W., Bodenhausen, G., Wagner, G. R., Ernst, R., and Wüthrich, K. (1983) *Biochem. Biophys. Res. Commun. 117*, 479−485.
34. Güntert, P., Dötsch, V., Wider, G., and Wüthrich, K. (1992) *J. Biomol. NMR 2*, 619−629.
35. Bartels, C., Xia, T. H., Billeter, M., Güntert, P., and Wüthrich, K. (1995) *J. Biomol. NMR 5*, 1−10.
36. Wüthrich, K. (1986) *NMR of Proteins and Nucleic Acids*, John Wiley and Sons Inc., New York.
37. Szyperski, T., Güntert, P., Otting, G., and Wüthrich, K. (1992) *J. Magn. Reson. 99*, 552−560.
38. Titman, J. J., and Keeler, J. (1990) *J. Magn. Reson. 89*, 640−646.
39. Güntert, P., Mumenthaler, C., and Wüthrich, K. (1997) *J. Mol. Biol. 273*, 283−298.
40. Bundi, A., and Wüthrich, K. (1979) *Biopolymers 18*, 285−297.
41. Merutka, G., Dyson, H. J., and Wright, P. (1995) *J. Biomol. NMR 5*, 14−24.
42. Merutka, G., Shalongo, W., and Stellwagen, E. (1991) *Biochemistry 30*, 4245−4248.
43. Duysens, L. N. M. (1956) *Biochim. Biophys. Acta 19*, 1−12.
44. Rizo, J., Blanco, F. J., Kobe, B., Bruch, M. D., and Gierasch, L. M. (1993) *Biochemistry 32*, 4881−4894.
45. Regan, L. (1995) *Trends Biol. Sci. 20*, 280−285.
46. Davies, S. M. A., Kelly, S. M., Price, N. C., and Bradshaw, J. P. (1998) *FEBS Lett. 425*, 415−418.
47. Brasseur, R., Pillot, T., Lins, L., Vanderkerckhove, J., and Rosseneu, M. (1997) *Trends Biol. Sci. 22*, 169−171.
48. Chang, D. K., Chien, W. J., and Chen, S. F. (1997) *Eur. J. Biochem. 247*, 896−905.
49. Koradi, R., Billeter, M., and Wüthrich, K. (1996) *J. Mol. Graphics 14*, 51−55.
50. Weber, T., Zemelman, B. V., McNew, J. A., Westermann, B., Gmachl, M., Parlati, F., Söllner, T. H., and Rothman, J. E. (1998) *Cell 92*, 759−772.

BI982130E